Instantaneous Bethe-Salpeter equation

M. G. Olsson and Siniša Veseli

Department of Physics, University of Wisconsin, Madison, Wisconsin 53706

Ken Williams

Continuous Electron Beam Accelerator Facility, Newport News, Virginia 29606
and Physics Department, Hampton University, Hampton, Virginia 29668

(Received 31 March 1995)

We present a systematic algebraic and numerical investigation of the instantaneous Bethe-Salpeter equation. Emphasis is placed on confining interaction kernels of the Lorentz scalar, time component vector, and full vector-types. We explore the stability of the solutions and Regge behavior for each of these interactions, and conclude that only time component vector confinement leads to normal Regge structure and stable solutions for all quark masses.

PACS number(s): 11.10.St, 11.55.Jy, 12.39.Pn

I. INTRODUCTION

The Bethe-Salpeter equation [1] follows from the general principles of quantum field theory [2]. The instantaneous form of the Bethe-Salpeter equation, known as the Salpeter equation [3], avoids difficulties related to the relative time degree of freedom and is believed to provide a firm framework for the discussion of bound state problems. Almost all knowledge of the solutions to the Salpeter equation is restricted to that sector where at least one of the constituent masses is large, in which case use of the so-called reduced Salpeter equation is justified. Relatively little work has been done on the algebraic properties [4–6] of the full Salpeter equation and even less on its numerical solution. A few years ago Lagaë [7] proposed a formalism that shows considerable promise for the systematic investigation of the full Salpeter equation. He also examined several confinement models [8] and concluded that the confining potential is not a scalar on the basis of nonlinear Regge behavior of the equal mass solutions. More recently, Münz *et. al.* [9] investigated a linear Lorentz scalar or alternatively a time component vector confining kernel combined with an effective interaction proposed by 't Hooft from instanton effects in QCD [10]. They found that there was no convincing parametrization for the confining kernel that leads to linear Regge trajectories and also yields spin-orbit terms of the correct sign. They also concluded that a scalar confining kernel does not lead to stationary solutions for higher angular momenta or small constituent masses. This conclusion inspired Parramore and Piekarewicz to perform a stability analysis of the variational solutions to the Salpeter equation in the pseudoscalar channel [11]. They concluded that time component vector confinement is stable with respect to the increase in the number of basis states, but they found the existence of imaginary eigenvalues for scalar confinement. One may argue though [12] that these authors have not considered the norm of the solutions in their analysis.

In this paper we extend Lagaë's method, correcting

a small but important algebraic error and exploring the full vector interaction kernel. We consider the nature of the solutions to the full Salpeter equation for interaction kernels of the time component Lorentz vector, scalar, and full vector types. The variational (Galerkin) method is used to investigate the reality of eigenvalues and the stability of the solutions with the above Lorentz interactions. We have taken the norm of the solutions into account in our analysis, since only states with a positive norm have direct physical significance. We have also investigated the Regge behavior for the above-mentioned kernels, and extended the analysis done in [8] to heavy-light systems. We also find that only the time component vector interaction leads to stable variational solutions and has normal Regge behavior. We should also emphasize at the outset that a time vector potential cannot be considered a realistic model of confinement, since it yields a spin-orbit interaction in conflict both with QCD and experiment.

This paper is organized as follows. In Sec. II we review some general properties of the Salpeter equation and the reduction to a system of coupled radial equations. The numerical results are discussed for each of the Lorentz kernels in Sec. III, and our conclusions are summarized in Sec. IV. Appendix A contains the complete coupled radial equations for the kernels considered in this paper, as well as a discussion of important limiting cases. The techniques of our numerical solution are covered in more detail in Appendix B.

II. REDUCTION TO RADIAL EQUATIONS

In this section we briefly review Lagaë's elegant formalism [7] for the reduction of the full Salpeter equation to a system of equations involving only radial wave functions. Our purpose here is to establish notation and to correct a small inconsistency in Lagaë's derivation, which, for example, leads to a couple of sign errors in the radial equations (5.7) of [7]. The correction does not affect the

equal mass case, which was the subject of Lagaë's numerical examples [8].

We start from the Salpeter equation for a fermion-antifermion system in the c.m. frame of the bound state:

$$M\chi = H_1\chi - \chi H_2 + \int \frac{d^3k'}{(2\pi)^3} V(\mathbf{k} - \mathbf{k}')$$

$$\times (\Lambda_+^1 \Gamma_1 \chi' \Gamma_2 \Lambda_-^2 - \Lambda_-^1 \Gamma_1 \chi' \Gamma_2 \Lambda_+^2) , \tag{1}$$

with the notation $f = f(\mathbf{k})$, $f' = f(\mathbf{k}')$. In the above equation $V(\mathbf{k} - \mathbf{k}')$ is a scalar function with Fourier transform $V(r)$ in the case of a Lorentz vector kernel, and $-V(r)$ in the case of a Lorentz scalar kernel. The Salpeter amplitude χ describing a mesonic bound state $|B\rangle$ is defined by

$$\chi(\mathbf{k}) = \langle 0|\psi_1(\mathbf{k})\psi_2^\dagger(\mathbf{k})|B\rangle , \tag{2}$$

Γ_1 and Γ_2 are 4×4 matrices corresponding to an interaction kernel with Lorentz structure $\gamma^0\Gamma_1 \otimes \gamma^0\Gamma_2$, while the H_i's and $\Lambda_\pm^i$'s are generalized Dirac Hamiltonians and energy projection operators, given by

$$H_i(\mathbf{k}) = A_i(\mathbf{k})\boldsymbol{\alpha} \cdot \hat{\mathbf{k}} + B_i(\mathbf{k})\beta , \tag{3}$$

$$\Lambda_\pm^i = \frac{E_i(\mathbf{k}) \pm H_i(\mathbf{k})}{2E_i(\mathbf{k})} , \tag{4}$$

with $E_i(\mathbf{k}) = \sqrt{A_i(\mathbf{k})^2 + B_i(\mathbf{k})^2}$. In this paper we restrict ourselves to constituent quarks of masses m_i, so that

$$A_i(\mathbf{k}) = k , \tag{5}$$

$$B_i(\mathbf{k}) = m_i , \tag{6}$$

$$E_i(\mathbf{k}) = \sqrt{m_i^2 + \mathbf{k}^2} . \tag{7}$$

Using properties of projection operators, it can be easily shown that the Salpeter amplitude satisfies the constraint condition

$$\frac{H_1}{E_1}\chi + \chi\frac{H_2}{E_2} = 0 . \tag{8}$$

Taking this into account, the norm of the Salpeter amplitude [4, 6] can be written as

$$||\chi||^2 = \int \frac{d^3k'}{(2\pi)^3}\text{Tr}\left[\chi^\dagger\frac{H_1}{E_1}\chi\right] \tag{9}$$

and is related to the normalization of bound states as

$$||\chi||^2 = \frac{1}{(2\pi)^3}\langle B|B\rangle . \tag{10}$$

Using (1) inside of (9) one obtains

$$M||\chi||^2 = \int \frac{d^3k}{(2\pi)^3}[E_1 + E_2]\,\text{Tr}[\chi^\dagger\chi]$$

$$+ \int \frac{d^3k}{(2\pi)^3}\int \frac{d^3k'}{(2\pi)^3}V(\mathbf{k} - \mathbf{k}')$$

$$\times\text{Tr}[\chi^\dagger\Gamma_1\chi'\Gamma_2] . \tag{11}$$

This equation will be used for obtaining radial equations from the variational principle as outlined in [7].

Now, if we expand the Salpeter amplitude as

$$\chi = \mathcal{L}_0 + \mathcal{L}_i\rho_i + \mathcal{N}_0 \cdot \boldsymbol{\sigma} + \mathcal{N}_i \cdot \rho_i\boldsymbol{\sigma} , \tag{12}$$

using 16 Hermitian matrices whose squares are unity $(1, \rho_i, \boldsymbol{\sigma}, \rho_i\boldsymbol{\sigma})$ as defined in [6], it is then easily seen that the constraint (8) can be satisfied by expressing the 16 components of χ ($\mathcal{L}$'s and $\mathcal{N}$'s) in terms of eight functions $(L_1, L_2, \mathbf{N}_1, \mathbf{N}_2)$ in the following way:

$$\begin{aligned}
\mathcal{L}_0 &= S_\theta(\hat{\mathbf{k}} \cdot \mathbf{N}_2) , \\
\mathcal{L}_1 &= S_\phi L_1 , \\
\mathcal{L}_2 &= iC_\theta L_2 , \\
\mathcal{L}_3 &= -C_\phi(\hat{\mathbf{k}} \cdot \mathbf{N}_1) , \\
\mathcal{N}_0 &= S_\theta L_2\hat{\mathbf{k}} + iC_\phi(\hat{\mathbf{k}} \times \mathbf{N}_2) , \\
\mathcal{N}_1 &= S_\phi\hat{\mathbf{k}}(\hat{\mathbf{k}} \cdot \mathbf{N}_1) - C_\theta\hat{\mathbf{k}} \times (\hat{\mathbf{k}} \times \mathbf{N}_1) , \\
\mathcal{N}_2 &= i[C_\phi\hat{\mathbf{k}}(\hat{\mathbf{k}} \cdot \mathbf{N}_2) - S_\phi\hat{\mathbf{k}} \times (\hat{\mathbf{k}} \times \mathbf{N}_2)] , \\
\mathcal{N}_3 &= -C_\phi L_1\hat{\mathbf{k}} - iS_\theta(\hat{\mathbf{k}} \times \mathbf{N}_1) .
\end{aligned} \tag{13}$$

Here we have used the notation

$$S_\phi = \sin\phi , \quad C_\phi = \cos\phi , \tag{14}$$

$$S_\theta = \sin\theta , \quad C_\theta = \cos\theta , \tag{15}$$

with angles ϕ and θ defined as

$$\phi = \frac{\phi_1 + \phi_2}{2} , \quad \theta = \frac{\phi_2 - \phi_1}{2} , \tag{16}$$

while the ϕ_i's are defined through

$$\cos\phi_i = \frac{A_i}{E_i} , \quad \sin\phi_i = \frac{B_i}{E_i} . \tag{17}$$

At this point we have departed from Lagaë in one small detail. Namely, we have redefined the function L_1 from Eq. (4.10) in [7], so that $L_1^{\text{our}} = -L_1^{\text{Lagaë}}$. The reason for doing so is that now, using (12) and (13) in the expression for the norm (9), one can obtain

$$||\chi||^2 = 4\int \frac{d^3k}{(2\pi)^3}[L_2^*(\mathbf{k})L_1(\mathbf{k}) + L_1^*(\mathbf{k})L_2(\mathbf{k})$$

$$+ \mathbf{N}_2^*(\mathbf{k}) \cdot \mathbf{N}_1(\mathbf{k}) + \mathbf{N}_1^*(\mathbf{k}) \cdot \mathbf{N}_2(\mathbf{k})] , \tag{18}$$

which is Eq. (4.13) from [7]. Using Lagaë's definition of L_1 would lead to minus signs in front of terms $L_2^*(\mathbf{k})L_1(\mathbf{k})$ and $L_1^*(\mathbf{k})L_2(\mathbf{k})$ in (18). This small inconsistency of Eqs. (4.10) and (4.13) from [7] leads to some incorrect signs in the final form of the radial equations for states with parity $P = (-1)^{J+1}$. In the equal mass case the terms with incorrect signs vanish, so that the numerical results obtained in [8] are not affected.

Now we proceed to obtain the radial equations. We first express L_i and $\mathbf{N}_i$ in terms of spherical harmonics and vector spherical harmonics (for an extensive discussion of generic wave functions and the identification of the quantum numbers of the bound states the reader is again referred to [7]), so that

$$L_i(\mathbf{k}) = L_i(k)Y_{JM}(\hat{\mathbf{k}}) , \tag{19}$$

$$\mathbf{N}_i(\mathbf{k}) = N_{i-}(k)\mathbf{Y}_-(\hat{\mathbf{k}})$$
$$+N_{i0}(k)\mathbf{Y}_0(\hat{\mathbf{k}}) + N_{i+}(k)\mathbf{Y}_+(\hat{\mathbf{k}}) , \tag{20}$$

where $\mathbf{Y}_-$, $\mathbf{Y}_0$, and $\mathbf{Y}_+$, stand for $\mathbf{Y}_{JJ-1M}$, $\mathbf{Y}_{JJM}$, and $\mathbf{Y}_{JJ+1M}$, respectively. We also introduce the functions n_{i+} and n_{i-}, defined as

$$\begin{bmatrix} n_{i+} \\ n_{i-} \end{bmatrix} = \begin{bmatrix} \mu & \nu \\ -\nu & \mu \end{bmatrix} \begin{bmatrix} N_{i+} \\ N_{i-} \end{bmatrix} , \tag{21}$$

with

$$\mu = \sqrt{\frac{J}{2J+1}} , \tag{22}$$

$$\nu = \sqrt{\frac{J+1}{2J+1}} . \tag{23}$$

Using these definitions, together with properties of spherical and vector spherical harmonics, we find, from (13),

$$\mathcal{L}_0 = S_\theta n_{2-} Y_{JM} ,$$
$$\mathcal{L}_1 = S_\phi L_1 Y_{JM} ,$$
$$\mathcal{L}_2 = iC_\theta L_2 Y_{JM} ,$$
$$\mathcal{L}_3 = -C_\phi n_{1-} Y_{JM} ,$$
$$\mathcal{N}_0 = C_\phi n_{2+} \mathbf{Y}_0 + (\nu C_\phi N_{20} + \mu S_\theta L_2)\mathbf{Y}_-$$
$$+(\mu C_\phi N_{20} - \nu S_\theta L_2)\mathbf{Y}_+ , \tag{24}$$
$$\mathcal{N}_1 = C_\theta N_{10} \mathbf{Y}_0 + (\mu S_\phi n_{1-} + \nu C_\theta n_{1+})\mathbf{Y}_-$$
$$+(-\nu S_\phi n_{1-} + \mu C_\theta n_{1+})\mathbf{Y}_+ ,$$
$$\mathcal{N}_2 = i[S_\phi N_{20} \mathbf{Y}_0 + (\nu S_\phi n_{2+} + \mu C_\theta n_{2-})\mathbf{Y}_-$$
$$+(\mu S_\phi n_{2+} - \nu C_\theta n_{2-})\mathbf{Y}_+] ,$$
$$\mathcal{N}_3 = -S_\theta n_{1+} \mathbf{Y}_0 + (-\mu C_\phi L_1 - \nu S_\theta N_{10})\mathbf{Y}_-$$
$$+(\nu C_\phi L_1 - \mu S_\theta N_{10})\mathbf{Y}_+ .$$

In the above formulas everything is expressed in terms of radial functions [e.g., $L_i = L_i(k)$, and so on]. Let us briefly review the quantum numbers of the states that these radial functions represent (parity P, charge conjugation C, and $^{2S+1}L_J$):

$$\begin{array}{llll} L_1, L_2, & P = (-1)^{J+1}, & C = (-1)^J, & {}^1J_J, \\ N_{10}, N_{20}, & P = (-1)^{J+1} & C = (-1)^{J+1}, & {}^3J_J, \\ n_{1+}, n_{2+}, n_{1-}, n_{2-}, & P = (-1)^J & C = (-1)^J, & {}^3(J \pm 1)_J. \end{array} \tag{25}$$

Substituting (24) in the expression for the norm (18), and using the angular integrals summarized in [7], we find

$$||\chi||^2 = 4 \int_0^\infty \frac{k^2 dk}{(2\pi)^3} [L_1^* L_2 + L_2^* L_1 + N_{10}^* N_{20} + N_{20}^* N_{10} + n_{1+}^* n_{2+} + n_{2+}^* n_{1+} + n_{1-}^* n_{2-} + n_{2-}^* n_{1-}] . \tag{26}$$

Similarly, for the kinetic energy part of (11) we get

$$\int \frac{d^3\mathbf{k}}{(2\pi)^3} [E_1 + E_2] \, \text{Tr}[\chi^\dagger(\mathbf{k})\chi(\mathbf{k})] = 4 \int_0^\infty \frac{k^2 dk}{(2\pi)^3} [E_1 + E_2]$$

$$\times [L_1^* L_1 + L_2^* L_2 + N_{10}^* N_{10} + N_{20}^* N_{20} + n_{1+}^* n_{1+} + n_{2+}^* n_{2+} + n_{1-}^* n_{1-} + n_{2-}^* n_{2-}] . \tag{27}$$

Each type of kernel must be treated separately. Here, for example, we give kernel part of (11) for the interaction of the form $\gamma^0 \otimes \gamma^0$ ($\Gamma_1 = \Gamma_2 = 1$):

$$\int \frac{d^3\mathbf{k}}{(2\pi)^3} \int \frac{d^3\mathbf{k}'}{(2\pi)^3} V(\mathbf{k} - \mathbf{k}') \, \text{Tr}[\chi^\dagger \Gamma_1 \chi' \Gamma_2] = 4(2\pi) \int_0^\infty \frac{k^2 dk}{(2\pi)^3} \int_0^\infty \frac{k'^2 dk'}{(2\pi)^3}$$

$$\times \Big\{ \; L_1^*[S_\phi V_J S_\phi' L_1' + C_\phi(\mu^2 V_{J-1} + \nu^2 V_{J+1})C_\phi' L_1' + \mu\nu C_\phi(V_{J-1} - V_{J+1})S_\theta' N_{10}']$$

$$+L_2^*[C_\theta V_J C_\theta' L_2' + S_\theta(\mu^2 V_{J-1} + \nu^2 V_{J+1})S_\theta' L_2' + \mu\nu S_\theta(V_{J-1} - V_{J+1})C_\phi' N_{20}']$$

$$+N_{10}^*[C_\theta V_J C_\theta' N_{10}' + S_\theta(\nu^2 V_{J-1} + \mu^2 V_{J+1})S_\theta' N_{10}' + \mu\nu S_\theta(V_{J-1} - V_{J+1})C_\phi' L_1']$$

$$+N_{20}^*[S_\phi V_J S_\phi' N_{20}' + C_\phi(\nu^2 V_{J-1} + \mu^2 V_{J+1})C_\phi' N_{20}' + \mu\nu C_\phi(V_{J-1} - V_{J+1})S_\theta' L_2'] \tag{28}$$

$$+n_{1+}^*[S_\theta V_J S_\theta' n_{1+}' + C_\theta(\nu^2 V_{J-1} + \mu^2 V_{J+1})C_\theta' n_{1+}' + \mu\nu C_\theta(V_{J-1} - V_{J+1})S_\phi' n_{1-}']$$

$$+n_{2+}^*[C_\phi V_J C_\phi' n_{2+}' + S_\phi(\nu^2 V_{J-1} + \mu^2 V_{J+1})S_\phi' n_{2+}' + \mu\nu S_\phi(V_{J-1} - V_{J+1})C_\phi' n_{2-}']$$

$$+n_{1-}^*[C_\phi V_J C_\phi' n_{1-}' + S_\phi(\mu^2 V_{J-1} + \nu^2 V_{J+1})S_\phi' n_{1-}' + \mu\nu S_\phi(V_{J-1} - V_{J+1})C_\theta' n_{1+}']$$

$$+n_{2-}^*[S_\theta V_J S_\theta' n_{2-}' + C_\theta(\mu^2 V_{J-1} + \nu^2 V_{J+1})C_\theta' n_{2-}' + \mu\nu C_\theta(V_{J-1} - V_{J+1})S_\phi' n_{2+}'] \; \Big\} ,$$

with V_L defined as

$$V_L(k, k') = 8\pi \int_0^\infty r^2 dr V(r) j_L(kr) j_L(k'r) . \quad (29)$$

At this point we can obtain the radial equations by taking variations of (26), (27), and (28), with respect to $L_1^*(k), L_2^*(k), \ldots, n_{2-}^*(k)$. The resulting equations for the $\gamma^0 \otimes \gamma^0$ kernel, as well as for the $\mathbf{1} \otimes \mathbf{1}$ and $\gamma^\mu \otimes \gamma_\mu$ kernels, are summarized in Appendix A.

Of course, one can also obtain these equations by straightforward substitution of (12) and (24) into the Salpeter equation (1) and then taking the trace after multiplication of the resulting equation with the appropriate matrices. The angular integrals that one needs can be worked out easily using the definition of vector spherical harmonics, the expression for $Y_{l_1}^{m_1}(\Omega) Y_{l_2}^{m_2}(\Omega)$, and the general properties of the Clebsch-Gordan coefficients, as given in Appendix C of [13]. However, Lagaë's method reviewed in this section is much more simple and elegant.

III. NUMERICAL RESULTS

As outlined in Appendix B, one solves the radial equations by expanding the wave functions in terms of a complete set of basis states, which depend on a variational parameter β. This expansion is then truncated to a finite number of basis states. In this way, a set of coupled radial equations can be transformed into a matrix equation, $\mathcal{H}\psi = M\psi$. The eigenvalues M of the matrix $\mathcal{H}$ will depend on β, and by looking for the extrema of $M(\beta)$ one can find the bound states. If the calculation is stable, increasing the number of basis states used will decrease the dependence of the eigenvalues on β. The regions of β with the same eigenvalues should thus enlarge.

A stability analysis of the variational solutions for the pseudoscalar states has been recently performed in [11]. Using the fact that the Salpeter equation can be cast in a form identical in structure to a random-phase-approximation equation, the authors of [11] have employed the same formalism developed by Thouless in his study of nuclear collective excitations [14], to perform a stability analysis of the Salpeter equation with Lorentz time component vector and scalar confining kernels. They find the presence of instability, manifested by the appearance of imaginary eigenvalues, in the case of scalar confinement. On the other hand, they find no such evidence in the case of time component vector confinement.

Since matrix $\mathcal{H}$ is not symmetric, its eigenvalues are not guaranteed to be real. However, as noted in [7, 15], the reality of eigenvalues follows from the reality of the norm and of the right-hand side of (11) when Γ_1 and Γ_2 are Hermitian, unless the norm is zero. Physically acceptable solutions must have a positive (and nonzero) norm. One may argue [12] that the authors of [11] have not taken this into account. Therefore, we find it worthwhile to examine the stability of the variational solutions to the Salpeter equation by taking the norm into account, i.e., by rejecting states with negative or zero norm. In the

following we consider the above issues for three different kernels, $\gamma^0 \otimes \gamma^0$, $\gamma^\mu \otimes \gamma_\mu$, and $\mathbf{1} \otimes \mathbf{1}$.

A. $\gamma^0 \otimes \gamma^0$ kernel (time component Lorentz vector)

The case of the $\gamma^0 \otimes \gamma^0$ confining kernel $(V(r) = ar)$ was found [11] to be stable with respect to an increase in the number of the basis states, even with very small quark masses. In order to verify this, we have performed a similar calculation for the pseudoscalar case $J^{PC} = 0^{-+}$, using $a = 0.2$ GeV^2 and zero mass quarks, with as many as 50 basis states. Results for the lowest three physical states (with positive norm) are shown in Fig. 1. One can see that, as the number of basis states increases, plateaus with the same eigenvalues enlarge, and there is no sign of instability. The same calculation was performed with states of higher angular momentum (even as high as $J = 20$), and again the results are the same. Therefore, we confirm the conclusion reached by the authors of [11] that the time component vector confinement is well behaved and suitable for a variational solution. As an additional check of our programs, we have reobtained all the numerical values for the time component vector confinement with several different quark masses, which are given in Table 1 of [11].

In Figs. 2 and 3 we show the leading and the first few daughter Regge trajectories in the case of $P = -C$ mesons in the light-light and heavy-light systems. As expected, we obtained slopes of $\frac{1}{8a}$ for the light-light, and $\frac{1}{4a}$ for the heavy-light systems.

In Fig. 4 we plot radial wave functions for the lowest-lying S and P waves in coordinate space. We have used $V(r) = ar$ $(a = 0.2$ GeV$^2)$ and zero mass quarks. The wave functions were normalized so that $||\chi||^2 = \frac{(2\pi)^3}{4}$.

Finally, it is a well-known fact that the Salpeter equa-
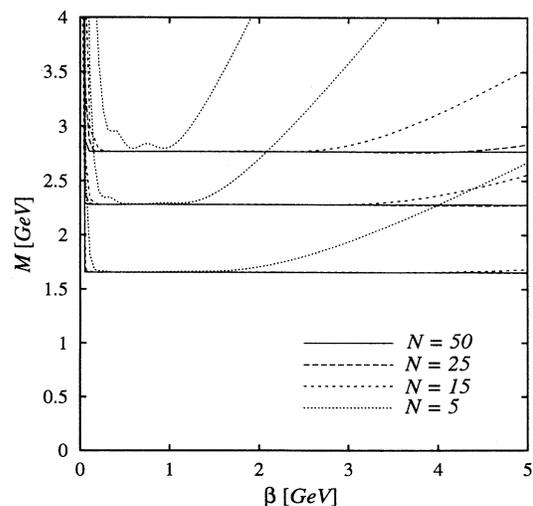
FIG. 1. The lowest three states with positive norm for time component vector confinement $[V(r) = ar, a = 0.2$ GeV$^2]$ in the pseudoscalar case, with $m_1 = m_2 = 0$. Calculations were done using 5, 15, 25, and 50 basis states.
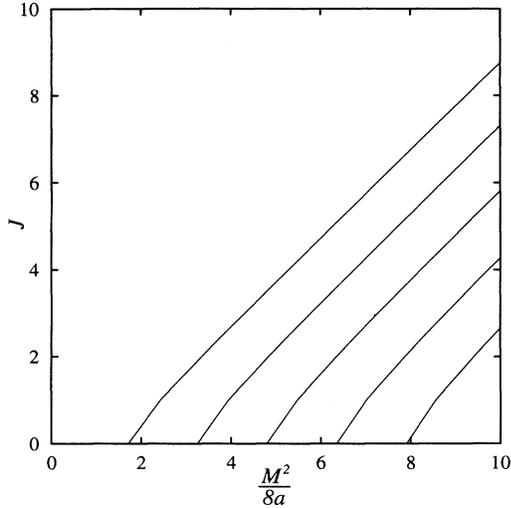
FIG. 2. Regge trajectories for a time component vector confinement $[V(r) = ar, a = 0.2 \text{ GeV}^2]$ in the light-light case with equal mass quarks $P = (-1)^{J+1}$ and $C = (-1)^J$. We have taken $m_1 = m_2 = 0$, and used 25 basis states.

FIG. 4. Radial wave functions in coordinate space for the $J^{PC} = 0^{-+}$ ($^1S_0$ state; L_1 is the lower and L_2 the upper full line), and $J^{PC} = 0^{++}$ ($^3P_0$ state; n_{1-} is the upper and n_{2-} the lower dashed line), with a time component vector kernel and $V(r) = ar$ ($a = 0.2 \text{ GeV}^2$). We have chosen quark masses $m_1 = m_2 = 0$. The calculation was done with 15 basis states.

tion does not reduce to the Dirac equation in the limit where one quark mass becomes infinite [16]. What is needed is an interaction that allows the existence of single-pair terms. These terms arise from kernels involving crossed ladder diagrams. Therefore, it is interesting to compare the exact solution of the Dirac equation with the time component vector Coulomb potential $[V(r) = -\frac{\kappa}{r}]$ with the solution of the Salpeter equation

in the heavy-light limit. In Fig. 5 we plot the Coulomb energy for these two equations as a function of the light quark mass and for three different values of κ. For example, for the light quark mass of $m_1 = 0.3$ GeV and for $\kappa = 0.75$ the effect is of the order of magnitude of 10 MeV. We note that for small m_1 this system becomes spatially large and weakly bound.

FIG. 3. Regge trajectories for a time component vector confinement $[V(r) = ar, a = 0.2 \text{ GeV}^2]$ in the heavy-light case with $P = (-1)^{J+1}$. We have taken $m_1 = 0$, $m_2 = 5.0$ GeV, and used 25 basis states in the equations corresponding to the heavy-light limit.
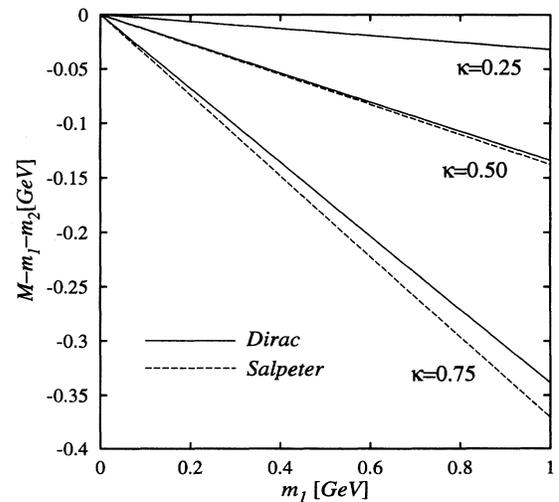
FIG. 5. Comparison of the Coulombic ground-state energy as a function of light quark mass m_1, obtained from the Dirac (full lines) and heavy-light Salpeter equation (dashed lines), with a time component vector Coulomb potential $[V(r) = -\frac{\kappa}{r}]$.

B. $1 \otimes 1$ kernel (Lorentz scalar)

As far as stability of the scalar confinement is concerned, things are completely different. The authors of [11] claim that imaginary eigenvalues occur as they increase the number of basis states, even for large values of the quark mass. For the particular choice of $m_1 = m_2 = 0.9$ GeV and $a = 0.29$ GeV^2 they find that increasing the number of basis states from 20 to 25 leads to the first occurrence of imaginary eigenvalues (for the pseudoscalar state). Using these parameters we find no imaginary eigenvalues, even with as many as 50 basis states. However, as shown in Fig. 6, scalar confinement in the full Salpeter equation does have a stability problem. As soon as basis states having large enough momentum components are included into the calculation, instabilities occur. As seen in Fig. 6, if one includes only 25 basis states, the three lowest states with positive norm have all well-defined plateaus in variational parameter β. But as soon as we go from 25 to 35 basis states, the third state with positive norm develops instability. Of course, for the ground state this instability occurs later. In order to see the magnitude of this effect, we have enlarged the scale for the behavior of the ground-state plateau in Fig. 7. As one can see, increasing the number of basis states from 39 to 40 leads to a decrease of energy in one small region of β. Naturally, these problems occur much earlier with smaller quark masses. To gain some insight into the nature of this instability, we show in Fig. 8 the behavior of the wave functions as the instability occurs. We have taken the same parameters as for the previous two figures and chosen $\beta = 1.538$ GeV (in the middle of the instability from Fig. 7). As one might expect, with 39 basis states the radial wave functions still preserve behavior characteristic of an S wave, which is lost for the

FIG. 7. The lowest pseudoscalar state with positive norm for scalar confinement $[V(r) = ar, a = 0.29$ GeV$^2]$ with $m_1 = m_2 = 0.9$ GeV. Calculations with 39 (dashed line) and 40 (full line) basis states are shown. This illustrates the onset of instability for this example of scalar confinement.

solutions with 40 basis states. It is also interesting to note that β near the edge of the unstable region (Fig. 7) yields wave functions that appear to be identical to the ones in the middle of it.

As far as imaginary eigenvalues obtained from the Salpeter equation with scalar confinement are concerned, we have indeed found these with very small quark masses. However, states with such eigenvalues always have a zero

FIG. 6. The lowest three states with positive norm for scalar confinement $(V(r) = ar, a = 0.29$ GeV$^2]$ in the pseudoscalar case, with $m_1 = m_2 = 0.9$ GeV. Calculations were done using 5, 25, and 35 basis states.
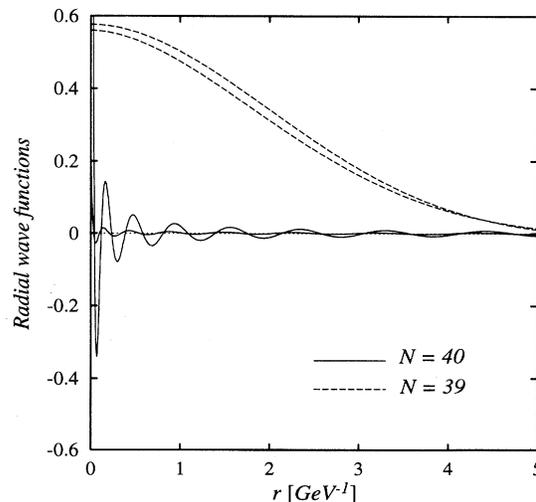
FIG. 8. Pseudoscalar ground-state radial wave functions L_1 and L_2 in coordinate space with a scalar confining kernel and $V(r) = ar$ $(a = 0.29$ GeV$^2)$. Quark masses were $m_1 = m_2 = 0.9$ GeV. Calculations with 39 (dashed line) and 40 (full line) basis states are shown, and the variational parameter was $\beta = 1.538$ GeV.

norm and have to be rejected. Therefore, in this case we do not agree with [11] and support conclusions reached by [7, 15] that physical states will have a positive norm and positive energies. However, we do agree with [11] that the Salpeter equation with scalar confinement does have a stability problem. Let us also briefly mention that if one squares the ground-state energy from Fig. 7, one obtains 6.750 GeV^2, a number to which the calculation of [11] converges before instability occurs (Table 2 in [11]). We do not want to speculate on the reasons why calculations done in [11] are much less stable than ours (for example, with parameters used for Figs. 6 and 7 we have not found imaginary eigenvalues even with 50 basis states, while there they already occur with 25 basis states). We might point out though that the pseudo-Coulombic basis functions we used here are much more suitable for the description of hadronic systems than harmonic oscillator basis functions used in [11].

We also confirm that there are problems with Regge trajectories with scalar confinement in the Salpeter equation as already found in [8, 17]. With large quark masses and a small number of basis states, we show in Fig. 9 that Regge trajectories are not linear. The situation is not improved even in the heavy-light limit, as can be seen in Fig. 10. We would like to point out that this can be easily understood from the so-called "no-pair" equation. The Salpeter equation and its reduced version in the heavy-light limit are the same as the no-pair equation [18], and for the no-pair equation with scalar confinement, it was shown analytically [19] that linear Regge behavior is lost. If the linear Regge behavior is lost in the heavy-light limit, one cannot expect that it will be restored when both quarks have finite mass.

Finally, let us just mention that we have also investigated the stability of a mixture of time component vector

FIG. 10. Regge trajectories for scalar confinement [$V(r) = ar$, $a = 0.2$ GeV^2] in the heavy-light case with $P = (-1)^{J+1}$. We have taken $m_1 = 0.1$ GeV, $m_2 = 5.0$ GeV, and used 25 basis states in the equations corresponding to the heavy-light limit.

and scalar confinement, i.e., for the kernels of the type

$$x\gamma^0 \otimes \gamma^0 + (1-x)\mathbf{1} \otimes \mathbf{1} \ . \tag{30}$$

This type of confining kernel (with $x = 0.5$), together with a one-gluon exchange kernel, was recently used in [20] for the investigation of the weak decays of B and D mesons. In order to illustrate this type of confinement, we show in Fig. 11 what happens as x goes from 0.49 to 0.51

FIG. 9. Regge trajectories for scalar confinement [$V(r) = ar$] with equal mass quarks and $P = (-1)^{J+1}$ and $C = (-1)^J$. We have taken $m_1 = m_2 = 1$ GeV, $a = 0.2$ GeV^2, and used 25 basis states.
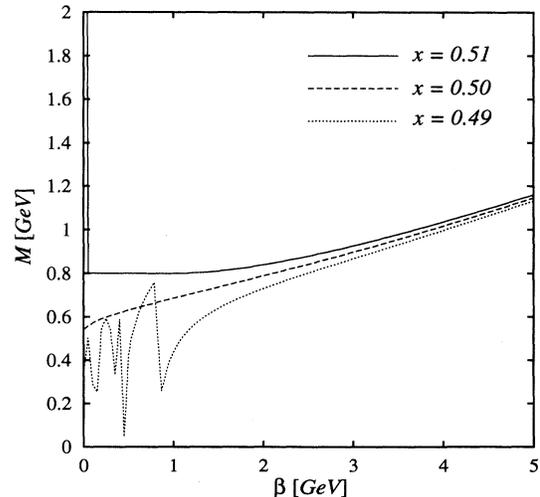
FIG. 11. The lowest state with positive norm for the mixture of time component vector and scalar confinement as given in (30) [$V(r) = ar$, $a = 0.2$ GeV^2, $m_1 = m_2 = 0$]. Calculations with $x = 0.51$ (full line), $x = 0.50$ (dashed line), and $x = 0.49$ (dotted line), correspond to 51%, 50%, and 49% of the time component vector kernel. We have used 15 basis states.
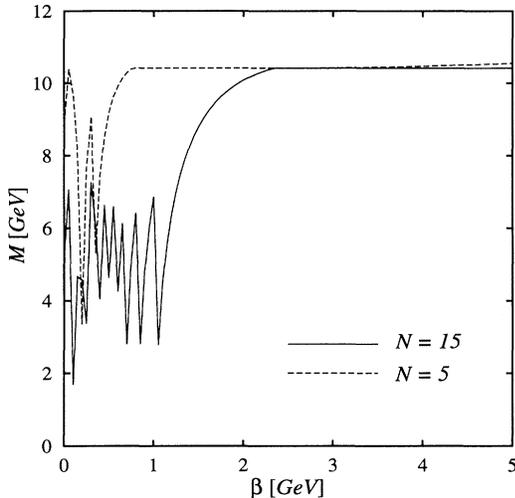
FIG. 12. The lowest state with positive norm for full Lorentz vector confinement $[V(r) = ar, a = 0.2 \text{ GeV}^2]$ in the pseudoscalar equal mass case, with the choice of $m_1 = m_2 = 5.0$ GeV. Calculations with 5 (dashed line) and 15 (full line) basis states are shown.

(with zero mass quarks and pure confining potential). Obviously, in this case solutions are stable only if $x > 0.5$. With the addition of a short-range Coulomb potential, variational solutions exist also for $x = 0.5$. A similar conclusion was also reached in [11].

C. $\gamma^\mu \otimes \gamma_\mu$ kernel (full Lorentz vector)

Full vector confinement behaves even worse than scalar confinement, as far as the variational method is concerned. As one can see in Fig. 12, the calculation is not stable even with quark masses as high as 5.0 GeV. Increasing the number of the basis states only makes things worse, as well as decreasing the quark mass. It is also interesting to note that this kernel exhibits similar problems even with a pure Coulomb potential, which was, on the other hand, found to be stable with scalar and time component vector kernels. Imaginary eigenvalues with this type of kernel are quite common, but again we emphasize that all such solutions have a zero norm and must be rejected.

IV. CONCLUSIONS

In this paper we have corrected a small inconsistency in Lagaë's derivation of the radial equations for the full Salpeter equation [7], and extended his analysis to the case of a full Lorentz vector kernel. We have concentrated here on the nature of variational solutions to the full Salpeter equation with a linear confining potential and three different types of kernels: time component vector, full vector, and Lorentz scalar. In each case we have examined the stability of variational solutions, and, when possible, the Regge structure in the equal mass and the heavy-light cases. Our results support previous conclusions that scalar confinement yields unstable varia-

tional solutions [11] and nonlinear Regge trajectories [8, 17], even in the heavy-light limit. On the other hand, the variational solutions for the time component vector confinement are stable and give linear Regge trajectories with the expected slopes for both the equal mass and heavy-light cases. In addition, we have found that variational solutions for full vector confinement are even more unstable than the ones for scalar confinement. We emphasize that our analysis took into account the norm of the solutions. Our numerical results completely support the theoretical conclusions of [8, 15] that eigenvalues for the states with physical norms are always real. Imaginary eigenvalues do appear, and are quite common for full vector confinement, but these solutions always have zero norm.

The occurrence of nonlinear Regge trajectories in scalar confinement is an extension of the results of Gara *et al.* [17] (for the reduced Salpeter equation) and Lagaë [8] (for the full Salpeter equation) in the equal mass case. We have found that the same problem persists even in the heavy-light case. The origin of this effect can be explained analytically from the so-called no-pair equation in coordinate space [19].

Even though the time component vector interaction behaves perfectly in the full Salpeter equation and leads to the expected linear Regge trajectories, it cannot be directly applied in any realistic meson model because it conflicts with QCD. The most evident example of this conflict is its wrong sign of the spin-orbit splitting.

ACKNOWLEDGMENTS

APPENDIX A: RADIAL EQUATIONS

In this appendix we give the complete set of radial equations for the kernels considered in this paper. These equations represent the general case of a quark with mass m_1 and an antiquark with mass m_2. One has to keep in mind that for $J = 0$ four wave functions vanish, i.e., we have $N_{10} = N_{20} = 0$ and $n_{1+} = n_{2+} = 0$.

In the equal mass case these equations somewhat simplify, since one has $E_1 = E_2$, $\phi = \phi_1 = \phi_2$, and $\theta = 0$, so that $S_\theta = 0$ and $C_\theta = 1$. Also, since charge conjugation is a good quantum number in the equal mass case, the four $P = (-1)^{J+1}$ state equations split into two systems of two equations, one corresponding to $C = (-1)^J$ (involving L_1 and L_2), and the other corresponding to $C = (-1)^{J+1}$ (involving N_{10} and N_{20}).

The heavy-light limit $(m_2 \to \infty)$ is obtained by setting $E_2 \to m_2$, $\phi_2 \to \frac{\pi}{2}$, so that $S_\theta \to C_\phi$ and $C_\theta \to S_\phi$. It is

interesting to note that in the heavy-light limit (and for kernels $\gamma^0 \otimes \gamma^0$ and $\mathbf{1} \otimes \mathbf{1}$, but not for the $\gamma^\mu \otimes \gamma_\mu$ kernel) physical solutions satisfy $L_1 = L_2$ and $N_{10} = N_{20}$ [for the $P = (-1)^{J+1}$ states], or $n_{1+} = n_{2+}$ and $n_{1-} = n_{2-}$ [for the $P = (-1)^J$ states]. Therefore, in these cases the system of four equations can be reduced to a system of only two radial equations.

Of course, for any mixture of different kernels, only the kernel parts of the radial equations should be added, and the kinetic energy terms are always the same. In the $\mathbf{1} \otimes \mathbf{1}$ case, we have introduced an additional minus sign in the kernel, so that $V(r)$ has the same form for all three cases considered, e.g. for the Cornell potential $V(r) = ar - \frac{\kappa}{r}$.

1. $\gamma^0 \otimes \gamma^0$ kernel

States with parity $P = (-1)^{J+1}$ are

$$ML_1 = [E_1 + E_2]L_2 + \int_0^\infty \frac{k'^2 dk'}{(2\pi)^2}[C_\theta V_J C_\theta' L_2' + S_\theta(\mu^2 V_{J-1} + \nu^2 V_{J+1})S_\theta' L_2' + \mu\nu S_\theta(V_{J-1} - V_{J+1})C_\phi' N_{20}'] \ ,$$

$$ML_2 = [E_1 + E_2]L_1 + \int_0^\infty \frac{k'^2 dk'}{(2\pi)^2}[S_\phi V_J S_\phi' L_1' + C_\phi(\mu^2 V_{J-1} + \nu^2 V_{J+1})C_\phi' L_1' + \mu\nu C_\phi(V_{J-1} - V_{J+1})S_\theta' N_{10}'] \ ,$$

$$\text{(A1)}$$

$$MN_{10} = [E_1 + E_2]N_{20} + \int_0^\infty \frac{k'^2 dk'}{(2\pi)^2}[S_\phi V_J S_\phi' N_{20}' + C_\phi(\nu^2 V_{J-1} + \mu^2 V_{J+1})C_\phi' N_{20}' + \mu\nu C_\phi(V_{J-1} - V_{J+1})S_\theta' L_2'] \ ,$$

$$MN_{20} = [E_1 + E_2]N_{10} + \int_0^\infty \frac{k'^2 dk'}{(2\pi)^2}[C_\theta V_J C_\theta' N_{10}' + S_\theta(\nu^2 V_{J-1} + \mu^2 V_{J+1})S_\theta' N_{10}' + \mu\nu S_\theta(V_{J-1} - V_{J+1})C_\phi' L_1'] \ .$$

States with parity $P = (-1)^J$ are

$$Mn_{1+} = [E_1 + E_2]n_{2+} + \int_0^\infty \frac{k'^2 dk'}{(2\pi)^2}[C_\phi V_J C_\phi' n_{2+}' + S_\phi(\nu^2 V_{J-1} + \mu^2 V_{J+1})S_\phi' n_{2+}' + \mu\nu S_\phi(V_{J-1} - V_{J+1})C_\theta' n_{2-}'] \ ,$$

$$Mn_{2+} = [E_1 + E_2]n_{1+} + \int_0^\infty \frac{k'^2 dk'}{(2\pi)^2}[S_\theta V_J S_\theta' n_{1+}' + C_\theta(\nu^2 V_{J-1} + \mu^2 V_{J+1})C_\theta' n_{1+}' + \mu\nu C_\theta(V_{J-1} - V_{J+1})S_\phi' n_{1-}'] \ ,$$

$$\text{(A2)}$$

$$Mn_{1-} = [E_1 + E_2]n_{2-} + \int_0^\infty \frac{k'^2 dk'}{(2\pi)^2}[S_\theta V_J S_\theta' n_{2-}' + C_\theta(\mu^2 V_{J-1} + \nu^2 V_{J+1})C_\theta' n_{2-}' + \mu\nu C_\theta(V_{J-1} - V_{J+1})S_\phi' n_{2+}'] \ ,$$

$$Mn_{2-} = [E_1 + E_2]n_{1-} + \int_0^\infty \frac{k'^2 dk'}{(2\pi)^2}[C_\phi V_J C_\phi' n_{1-}' + S_\phi(\mu^2 V_{J-1} + \nu^2 V_{J+1})S_\phi' n_{1-}' + \mu\nu S_\phi(V_{J-1} - V_{J+1})C_\theta' n_{1+}'] \ .$$

2. $\mathbf{1} \otimes \mathbf{1}$ kernel

States with parity $P = (-1)^{J+1}$ are

$$ML_1 = [E_1 + E_2]L_2 + \int_0^\infty \frac{k'^2 dk'}{(2\pi)^2}[C_\theta V_J C_\theta' L_2' - S_\theta(\mu^2 V_{J-1} + \nu^2 V_{J+1})S_\theta' L_2' - \mu\nu S_\theta(V_{J-1} - V_{J+1})C_\phi' N_{20}'] \ ,$$

$$ML_2 = [E_1 + E_2]L_1 + \int_0^\infty \frac{k'^2 dk'}{(2\pi)^2}[S_\phi V_J S_\phi' L_1' - C_\phi(\mu^2 V_{J-1} + \nu^2 V_{J+1})C_\phi' L_1' - \mu\nu C_\phi(V_{J-1} - V_{J+1})S_\theta' N_{10}'] \ ,$$

$$\text{(A3)}$$

$$MN_{10} = [E_1 + E_2]N_{20} + \int_0^\infty \frac{k'^2 dk'}{(2\pi)^2}[S_\phi V_J S_\phi' N_{20}' - C_\phi(\nu^2 V_{J-1} + \mu^2 V_{J+1})C_\phi' N_{20}' - \mu\nu C_\phi(V_{J-1} - V_{J+1})S_\theta' L_2'] \ ,$$

$$MN_{20} = [E_1 + E_2]N_{10} + \int_0^\infty \frac{k'^2 dk'}{(2\pi)^2}[C_\theta V_J C_\theta' N_{10}' - S_\theta(\nu^2 V_{J-1} + \mu^2 V_{J+1})S_\theta' N_{10}' - \mu\nu S_\theta(V_{J-1} - V_{J+1})C_\phi' L_1'] \ .$$

States with parity $P = (-1)^J$ are

$$Mn_{1+} = [E_1 + E_2]n_{2+} + \int_0^\infty \frac{k'^2 dk'}{(2\pi)^2}[-C_\phi V_J C_\phi' n_{2+}' + S_\phi(\nu^2 V_{J-1} + \mu^2 V_{J+1})S_\phi' n_{2+}' + \mu\nu S_\phi(V_{J-1} - V_{J+1})C_\theta' n_{2-}'] \ ,$$

$$Mn_{2+} = [E_1 + E_2]n_{1+} + \int_0^\infty \frac{k'^2 dk'}{(2\pi)^2} [-S_\theta V_J S'_\theta n'_{1+} + C_\theta(\nu^2 V_{J-1} + \mu^2 V_{J+1})C'_\theta n'_{1+} + \mu\nu C_\theta(V_{J-1} - V_{J+1})S'_\phi n'_{1-}] ,$$

$$(A4)$$

$$Mn_{1-} = [E_1 + E_2]n_{2-} + \int_0^\infty \frac{k'^2 dk'}{(2\pi)^2} [-S_\theta V_J S'_\theta n'_{2-} + C_\theta(\mu^2 V_{J-1} + \nu^2 V_{J+1})C'_\theta n'_{2-} + \mu\nu C_\theta(V_{J-1} - V_{J+1})S'_\phi n'_{2+}] ,$$

$$Mn_{2-} = [E_1 + E_2]n_{1-} + \int_0^\infty \frac{k'^2 dk'}{(2\pi)^2} [-C_\phi V_J C'_\phi n'_{1-} + S_\phi(\mu^2 V_{J-1} + \nu^2 V_{J+1})S'_\phi n'_{1-} + \mu\nu S_\phi(V_{J-1} - V_{J+1})C'_\theta n'_{1+}] .$$

3. $\gamma^\mu \otimes \gamma_\mu$ kernel

States with parity $P = (-1)^{J+1}$ are

$$ML_1 = [E_1 + E_2]L_2 + \int_0^\infty \frac{k'^2 dk'}{(2\pi)^2} [4C_\theta V_J C'_\theta L'_2 + 2S_\theta(\mu^2 V_{J-1} + \nu^2 V_{J+1})S'_\theta L'_2 + 2\mu\nu S_\theta(V_{J-1} - V_{J+1})C'_\phi N'_{20}] ,$$

$$ML_2 = [E_1 + E_2]L_1 + \int_0^\infty \frac{k'^2 dk'}{(2\pi)^2} [-2S_\phi V_J S'_\phi L'_1] ,$$

$$(A5)$$

$$MN_{10} = [E_1 + E_2]N_{20} + \int_0^\infty \frac{k'^2 dk'}{(2\pi)^2} [2C_\phi(\nu^2 V_{J-1} + \mu^2 V_{J+1})C'_\phi N'_{20} + 2\mu\nu C_\phi(V_{J-1} - V_{J+1})S'_\theta L'_2] ,$$

$$MN_{20} = [E_1 + E_2]N_{10} + \int_0^\infty \frac{k'^2 dk'}{(2\pi)^2} [2C_\theta V_J C'_\theta N'_{10}] .$$

States with parity $P = (-1)^J$ are

$$Mn_{1+} = [E_1 + E_2]n_{2+} + \int_0^\infty \frac{k'^2 dk'}{(2\pi)^2} [2C_\phi V_J C'_\phi n'_{2+}] ,$$

$$Mn_{2+} = [E_1 + E_2]n_{1+} + \int_0^\infty \frac{k'^2 dk'}{(2\pi)^2} [2C_\theta(\nu^2 V_{J-1} + \mu^2 V_{J+1})C'_\theta n'_{1+} + 2\mu\nu C_\theta(V_{J-1} - V_{J+1})S'_\phi n'_{1-}] ,$$

$$(A6)$$

$$Mn_{1-} = [E_1 + E_2]n_{2-} + \int_0^\infty \frac{k'^2 dk'}{(2\pi)^2} [-2S_\theta V_J S'_\theta n'_{2-}] ,$$

$$Mn_{2-} = [E_1 + E_2]n_{1-} + \int_0^\infty \frac{k'^2 dk'}{(2\pi)^2} [4C_\phi V_J C'_\phi n'_{1-} + 2S_\phi(\mu^2 V_{J-1} + \nu^2 V_{J+1})S'_\phi n'_{1-} + 2\mu\nu S_\phi(V_{J-1} - V_{J+1})C'_\theta n'_{1+}] .$$

APPENDIX B: NUMERICAL SOLUTION OF THE RADIAL EQUATIONS

As briefly mentioned in Sec. III, the easiest way to solve the radial equations given in Appendix A is to expand the radial wave functions $f(k)$ in terms of some complete set of basis functions $\{e_{iL}(k)\}$, and to truncate the expansion to the first N basis states, i.e.,

$$f(k) \simeq \sum_{i=0}^{N-1} c_i^f e_{iL}(k) . \qquad (B1)$$

In this way a set of n coupled radial equations becomes the $nN \times nN$ matrix equation

$$\mathcal{H}\psi = M\psi , \qquad (B2)$$

where ψ is an nN-dimensional vector:

$$\psi = \begin{pmatrix} f_1 \\ \vdots \\ f_n \end{pmatrix} . \qquad (B3)$$

The matrix $\mathcal{H}$ and its eigenvalues depend on the variational parameter β characterizing the basis functions. However, if the calculation is stable, dependence of the solution on β should reduce as N increases. This is manifested by the development of plateaus in β having the same eigenvalues.

A basis set that was shown to be very successful in calculations of this sort is given by [21]

$$e_{iL}(\beta, k) = (-i)^L \tilde{N}_{iL}\beta^{\frac{1}{2}} \left(\frac{\beta}{\beta^2 + k^2}\right)^{L+2}$$
$$\times k^L P_i^{(L+\frac{3}{2}, L+\frac{1}{2})} \left(-\left(\frac{k^2 - \beta^2}{k^2 + \beta^2}\right)\right) , \qquad (B4)$$

where $P_i^{(a,b)}(x)$ are Jacobi polynomials and

$$\tilde{N}_{iL} = \frac{2\Gamma(\frac{1}{2})}{\Gamma(i + L + \frac{3}{2})} \left[\frac{i!(i + 2L + 2)!}{\pi}\right]^{\frac{1}{2}} . \qquad (B5)$$

The Fourier transform of (B4) is known analytically,

$$e_{iL}(\beta, r) = N_{iL}\beta^{\frac{3}{2}} (2\beta r)^L e^{-\beta r} L_i^{(2L+2)}(2\beta r) , \qquad (B6)$$

with $L_i^{(a)}(x)$ being the generalized Laguerre polynomials and

$$N_{iL} = \left[\frac{8(i!)}{(i+2L+2)!}\right]^{\frac{1}{2}} . \tag{B7}$$

The kinetic energy terms of the $\mathcal{H}$ matrix (dropping the dependence of the basis states on β),

$$\int_0^\infty k^2 dk e_{iL}^*(k)\sqrt{k^2+m^2}\, e_{jL}(k) , \tag{B8}$$

can be efficiently calculated using the Gauss-Jacobi quadrature formula after performing a change of integration variable to $x = \frac{k^2-\beta^2}{k^2+\beta^2}$. Keeping in mind definition (29), the kernel part of $\mathcal{H}$ will in general include terms such as

$$\frac{2}{\pi}\int_0^\infty k^2 dk \int_0^\infty k'^2 dk' \int_0^\infty r^2 dr e_{iL}^*(k)$$

$$F(k)j_{L'}(kr)V(r)j_{L'}(k'r)G(k')e_{jL}(k') , \tag{B9}$$

where F and G are some functions of k and k', respectively. It is quite difficult to approximate these integrals by applying standard numerical quadrature methods, since the range of integration is infinite, and spherical Bessel functions $j_l(kr)$ are rapidly oscillating. In addition, we would have to perform the quadrature for each value of r where $V(r)j_{L'}(kr)j_{L'}(k'r)$ is needed. Therefore, it is much better to expand $F(k)e_{iL}(k)$ in terms of basis functions $\{e_{i'L'}\}$ [22], i.e.,

$$F(k)e_{iL}(k) \simeq \sum_{i'=0}^{N'-1} c_{i'i}^{(F,L',L)} e_{i'L'}(k) , \tag{B10}$$

where N' is the number of basis states of $\{e_{i'L'}\}$ used [similarly we have to expand $G(k')e_{jL}(k')$]. Now, the radial Fourier transforms

$$e_{iL}(r) = i^L \frac{4\pi}{(2\pi)^{\frac{3}{2}}} \int_0^\infty k^2 dk j_L(kr)e_{iL}(k) \tag{B11}$$

allow us to perform integrations over k and k' analytically, so that (B9) becomes

$$\sum_{i'=0}^{N'-1}\sum_{j'=0}^{N'-1} c_{i'i}^{(F,L',L)*} V_{i'j'}^{(L')} c_{j'j}^{(G,L',L)} , \tag{B12}$$

where

$$c_{i'i}^{(F,L',L)} = \int_0^\infty k^2 dk e_{i'L'}^*(k)F(k)e_{iL}(k) , \tag{B13}$$

$$V_{i'j'}^{(L')} = \int_0^\infty r^2 dr e_{i'L'}^*(r)V(r)e_{j'L'}(r) . \tag{B14}$$

Again, the integrals involved in the calculation of $c_{i'i}^{(F,L,L')}$ can be efficiently evaluated using the Gauss-Jacobi quadrature formula, while matrix elements of $V(r)$ were calculated analytically [19] for the short-range Coulomb and linear confining potential that were used in this paper.

In practice, we choose L in such a way that $L = J$ for the states with parity $P = (-1)^{J+1}$, and $L = J-1$ for the states with parity $P = (-1)^J$ (unless $J = 0$, when we take $L = 1$). From the radial equations given in Appendix A one can see that L' can take values $J-1$, J, or $J+1$, and we have found that generally taking $N' = 2N$ is more than enough to accurately describe all functions of the form $F(k)e_{iL}(k)$.

In order to make sure that numerical calculations were done correctly, we have written two independent programs, each of them treating the general (unequal mass) case, and also two limiting cases (equal mass and heavy-light limit) separately, for all kernels considered in the text. In addition to the consistency of the two programs of ours, and consistency of the two special cases with the general case, we have also checked our results against those of [8], where only equal mass case was considered, and of [11], where stability of pseudoscalar case was considered.

[1] E. E. Salpeter and H. A. Bethe, Phys. Rev. **76**, 1232 (1949).

[2] M. Gell-Mann and F. Low, Phys. Rev. **84**, 350 (1951).

[3] E. E. Salpeter, Phys. Rev. **87**, 328 (1952).

[4] C. H. Llewellyn Smith, Ann. Phys. (N.Y.) **53**, 521 (1969).

[5] T. Murota, Prog. Theor. Phys. **69**, 181 (1983).

[6] A. Le Yaouanc, L. Oliver, S. Ono, O. Pène, and J.-C. Raynal, Phys. Rev. D **31**, 137 (1985).

[7] J.-F. Lagaë, Phys. Rev. D **45**, 305 (1992).

[8] J.-F. Lagaë, Phys. Rev. D **45**, 317 (1992).

[9] C. R. Münz, J. Resag, B. C. Metsch, and H. R. Petry, Nucl. Phys. **A578**, 418 (1994).

[10] G. 't Hooft, Phys. Rev. D **14**, 3432 (1976); M. A. Shifman, A. I. Vainshtein, and V. I. Zakharov, Nucl. Phys. **B163**, 46 (1980); H. R. Petry et al., Phys. Lett. **159B**, 363 (1985).

[11] J. Parramore and J. Piekarewicz, Nucl. Phys. **A585**, 705 (1995).

[12] J.-F. Lagaë (private communication).

[13] A. Messiah, *Quantum Mechanics* (Wiley, New York,

1976), Vol. II.

[14] D. J. Thouless, Nucl. Phys. **21**, 225 (1960); **22**, 78 (1961).

[15] J. Resag, C. R. Münz, B. C. Metsch, and H. R. Petry, Nucl. Phys. **A578**, 397 (1994).

[16] See, for example, footnote 14 in S. J. Brodsky and J. R. Primack, Ann. Phys. **52**, 315 (1969), which refers to a private communication by D. R. Yennie.

[17] A. Gara, B. Durand, L. Durand, and L. J. Nickisch, Phys. Rev. D **40**, 843 (1989); A. Gara, B. Durand, and L. Durand, *ibid.* **42**, 1651 (1990).

[18] C. Long and D. Robson, Phys. Rev. D **27**, 644 (1983).

[19] M. G. Olsson, S. Veseli, and K. Williams, Phys. Rev. D **51**, 5079 (1995).

[20] G. Zöller, S. Hainzl, C. R. Münz, and M. Beyer, *Weak Decays of Heavy Mesons in the Instantaneous Bethe-Salpeter Approach*, Bonn University Report No. BONN-TK-94-15 (hep-ph/9412355).

[21] E. J. Weniger, J. Math. Phys. **26**, 276 (1985).

[22] S. Jacobs, Ph.D. thesis, University of Wisconsin at Madison, 1985.